White Rose Research Online

eprints@whiterose.ac.uk
https://eprints.whiterose.ac.uk
Universities of Leeds, Sheffield and York

Deposited via The University of York.

White Rose Research Online URL for this paper:
https://eprints.whiterose.ac.uk/id/eprint/150950/

Version: Published Version

Article:
Sims, Mark Timothy, Abbott, Laurence Colin, Goodby, John William et al. (2019) Shape segregation in molecular organisation: a combined X-ray scattering and molecular dynamics study of smectic liquid crystals. Soft Matter. ISSN: 1744-683X

https://doi.org/10.1039/C9SM01527B

Reuse
This article is distributed under the terms of the Creative Commons Attribution (CC BY) licence. This licence allows you to distribute, remix, tweak, and build upon the work, even commercially, as long as you credit the authors for the original work. More information and the full terms of the licence here: https://creativecommons.org/licenses/

Takedown
If you consider content in White Rose Research Online to be in breach of UK law, please notify us by emailing eprints@whiterose.ac.uk including the URL of the record and the reason for the withdrawal request.

UNIVERSITY OF LEEDS
University of Sheffield
UNIVERSITY of York

Soft Matter

PAPER

View Article Online
View Journal

Check for updates

Cite this: DOI: 10.1039/c9sm01527b

Shape segregation in molecular organisation: a combined X-ray scattering and molecular dynamics study of smectic liquid crystals†

Mark T. Sims, ‡ Laurence C. Abbott, John W. Goodby and John N. Moore *

Temperature-dependent X-ray scattering studies have been carried out on 4-undecyloxy-4′-cyanobiphenyl (11OCB) and 4-(12,12-dimethyltridecyloxy)-4′-cyanobiphenyl (*t*-Bu-11OCB) in the smectic A phase, from which their layer spacings and translational order parameters were obtained. Marked differences between the layer structures of the two compounds were demonstrated, showing that the addition of the *t*-Bu group results in a higher translational order parameter and wider layer spacing for *t*-Bu-11OCB than 11OCB. Fully atomistic MD simulations of both compounds run for >1000 ns demonstrated the spontaneous formation of smectic mesophases from isotropic starting geometries, and experimental trends in order parameters and absolute layer spacings were shown to be replicated well. Further analysis showed that both the aromatic head-groups and the alkyl tail-groups exhibit interdigitation in the simulated smectic phases of both compounds, and the difference in the layer structures between 11OCB and *t*-Bu-11OCB could be attributed mainly to a shape segregation effect arising from the addition of the bulky *t*-Bu end-group to the alkyl chain.

Received 29th July 2019,
Accepted 18th August 2019

DOI: 10.1039/c9sm01527b

rsc.li/soft-matter-journal

Open Access Article. Published on 11 September 2019. Downloaded on 9/17/2019 10:02:02 AM.
This article is licensed under a Creative Commons Attribution 3.0 Unported Licence.

Introduction

Smectic liquid crystal phases are characterised as those that exhibit both orientational and translational order, *i.e.* molecules within the phase have a tendency to align along a preferred orientation and also to self-organise into diffuse layers. The potential applications of smectic phases are widespread, and they may be found in a number of different types of display devices,[1–3] which can offer differing and in many cases favourable properties compared with more conventional devices based on nematic liquid crystal phases. As with any liquid crystal device, the tuning of the properties of the materials used within these devices is crucial to optimise their performance.

Of the subclasses of smectic phases, the simplest is the uniaxial smectic A (SmA) phase, in which the molecules organise into layers with layer-normal vectors coincident with the preferred molecular orientation. The smectic A phase has received significant attention because of the ability to use it in ion-doped systems to produce bistable displays that act in light-scattering mode,[4–6] and also in flexible displays.[7,8] In the context of display applications, the chiral smectic C (SmC*) phase, in which the molecules are tilted with respect to the layer normals, is perhaps the most studied because it may exhibit ferroelectric behaviour under suitable confinement conditions, enabling rapid switching of the molecular orientations to give extremely fast response times.[9] Although compounds exhibiting SmA and SmC* phases may both be found in commercial displays, there are material properties that limit their use. For example, defect-free domains are typically required in optical devices,[10] and layer instabilities are problematic for many applications of SmC* materials.[11] Additionally in SmA devices, the nature of the layer structure has a large impact on the conductivity anisotropy of ion-doped systems, influencing their threshold switching voltages.[12] Hence, a detailed understanding of the relationship between the structures of the constituent molecules and the layer structures within smectic phases is vital to overcoming issues with defect formation and performance in smectic devices.[13,14] Furthermore, understanding the response of the layer structure to external forces is crucial for the development of practical flexible displays.[15]

A significant amount of research has been carried out with the aim of optimising smectic materials for display applications, and in particular the effects of molecular structure on smectic phase stability and layer formation have been studied. One particular area of interest has been the influence of bulky end-groups, and a whole range of different effects have been reported. For example, an early study of chlorosilane-terminated liquid crystals proposed that the bulky polar end-groups favour smectic mesophases when compared with their alkyl-terminated analogues,[16] but later studies suggested that smectic phases are destabilised by the addition of epoxy[17] and halogen[18] end-groups.

Department of Chemistry, University of York, Heslington, York YO10 5DD, UK. E-mail: john.moore@york.ac.uk

† Electronic supplementary information (ESI) available. See DOI: 10.1039/c9sm01527b

‡ Current address: Department of Applied Sciences, Faculty of Health and Life Sciences, Northumbria University, Newcastle Upon Tyne, NE1 8ST, UK.

Open Access Article. Published on 11 September 2019. Downloaded on 9/17/2019 10:02:02 AM.
This article is licensed under a Creative Commons Attribution 3.0 Unported Licence.

Phenoxy end-groups have been reported to suppress SmC phases,[19] and the positions of fluorine substituents on phenoxy end-groups have been shown to influence the relative stabilities of the SmA and SmC phases.[20] In some cases, bulky non-polar end-groups have been proposed to preclude liquid-crystalline phases[16] and weaken interlayer interactions[21] due to their volume, but other studies have suggested that such groups may increase the temperature range over which the SmA phase is stable,[18] or enhance the stability of the SmC phase over the SmA phase.[22] It has also been reported that SmC stabilisation by bulky non-polar groups may only occur if the bulky group is not too large.[23] This range of effects arising from altering the steric and electrostatic properties of the end-groups illustrates the complexity in terms of phase structure and behaviour arising from relatively subtle changes in molecular structure, and demonstrates a need for improved understanding of structure–property relationships in this field.

Perhaps the most studied and well understood class of smectic liquid crystals is that of the interdigitated SmA_d phase formed by cyanobiphenyl molecules, in which there is significant overlap of molecules between the layers. The driving force for the formation of this phase has been attributed primarily to the dichotomy of the molecules, which favours self-association of the polarizable, polar cyanobiphenyl groups and of the non-polar aliphatic chains, resulting in chemically distinct regions in the layers.[24] This separation on a molecular scale is termed nanosegregation, and it is the nature of this effect that determines the exact structure of the phases exhibited by these compounds. The favoured antiparallel molecular configuration of neighbouring molecules combined with nanosegregation enables material properties such as the layer spacing of *ca.* 1.4 times the molecular length in cyanobiphenyl compounds to be rationalised.[25]

The influence of bulky end-groups on the properties of the smectic phases of cyanobiphenyls has been studied, with much work focusing on bulky siloxane end-groups.[26] These groups have been reported to promote layer formation, and this effect has been attributed primarily to the additional chemical incompatibility of the siloxane groups with both the aliphatic and aromatic regions of the molecules.[26,27] This reported three-way chemical incompatibility has been widely used to explain phase behaviour and material properties of siloxane-terminated cyanobiphenyls,[28–33] such as their small degree of out-of-layer fluctuations.[34] One of the primary reasons these compounds have been studied is the favourable threshold switching voltages and response times of mixtures comprising these compounds in devices.[35] Molecular theories of these materials based on nanosegregation promoting translational order have also been developed.[36]

However, this additional chemically driven nanosegregation in liquid crystals with bulky siloxane end-groups has been called into question as a result of similar properties being exhibited by mesogens with bulky alkyl end-groups,[18,37] suggesting that steric effects may be dominant. Although steric interactions were thought to be important in early work on siloxanes, these interactions were not considered to be the driving force behind the formation and properties of their smectic phases.[26] It appears that some of the discussion of nanosegregation within low molecular weight liquid crystals may originate from segregation in di-block copolymers comprising aromatic and siloxane units;[27,38] however, in compounds of low molecular weight these units have been shown to be miscible,[39] and low molecular weight polydimethylsiloxane oligomers have also been shown to be soluble in both aromatic and aliphatic solvents.[40] These apparently conflicting aspects of interpretation and observed behaviour raise questions over whether the material properties of siloxane-substituted liquid-crystalline systems originate primarily from the chemical or the topological properties of the molecules.

The range of effects reported for bulky end-groups, polar end-groups, and potentially chemically incompatible end-groups demonstrates a high degree of complexity in rationalising the properties of smectic phases, and raises fundamental questions relating to the driving forces of self-organisation. Quantitative conclusions at an atomic level are not readily obtained from experimental studies, but would provide an important route towards understanding the subtleties of self-organisation processes and ultimately to designing smectic materials with specific properties.

Molecular dynamics (MD) simulations provide a potential route towards such atomic-level understanding, and united-atom and fully-atomistic molecular dynamics simulations of thermotropic liquid crystals are becoming increasingly widespread as computational power increases and force-fields are developed and improved. The nematic phase has been the subject of many of these studies due to its relative simplicity, and research has typically focused on replicating and rationalising many experimental observables such as orientational order parameters, transition temperatures, densities, diffusion coefficients, molecular conformations and molecular associations.[41–44] Simulations of smectic phases provide a significantly greater challenge than nematic phases, largely as a result of the long-range translational order they exhibit, which preferably requires correspondingly large simulations that result in long computation times. Early united-atom and fully-atomistic simulations of smectic phases were therefore limited to <10 ns simulations of up to *ca.* 100 molecules,[45–48] providing only limited information on the smectic phase structure. The more recent ability to simulate larger systems of up to a few thousand molecules has prompted investigations into a wide range of systems exhibiting smectic phases, such as semi-fluorinated alkanes,[49,50] azobenzene-containing moieties,[51] and large aromatic species such as sexithiophene[52,53] and quinquephenyl.[54]

A significant focus of MD studies has also been on force field parameterisation and verification, most commonly for the ubiquitous cyanobiphenyl-based liquid crystals, enabling experimental transition temperatures, orientational order parameters, and translational order parameters of the smectic phases to be replicated.[43,55–60] Force-fields that have been parameterised for specific families of liquid-crystalline compounds unsurprisingly tend to replicate experimental properties somewhat better than general force fields, but depending on the method of parameterisation this may be at the significant cost of losing transferability to other families of compounds, limiting their use in a predictive context. Conversely,

 This journal is © The Royal Society of Chemistry 2019

Open Access Article. Published on 11 September 2019. Downloaded on 9/17/2019 10:02:02 AM.
This article is licensed under a Creative Commons Attribution 3.0 Unported Licence.

general force fields are typically less capable of predicting absolute experimental values, but nevertheless may successfully predict experimental trends, providing a valuable predictive method for tuning properties. Recently, adjustments to the General Amber Force Field (GAFF) have been shown to give a significant improvement in the prediction of transition temperatures, potentially providing a general atomistic force field suitable for the simulation of liquid crystal phases.[61]

In this work, our aim was to investigate the role of steric effects in the self-organisation of smectic liquid crystals through a combination of experimental X-ray scattering studies and fully atomistic MD simulations. As described above, much of the work on cyanobiphenyl compounds with bulky end-groups has focused on siloxane-containing moieties, but a comparison between alkyl- and siloxane-terminated molecules would not readily provide a distinction between chemically driven and sterically driven effects. Furthermore, molecules containing silicon may currently present a challenge for MD simulations because relatively little parameterisation has been carried out to date for silicon-containing species. In this work, we therefore chose to study two alkyl-terminated cyanobiphenyl compounds; one straight-chain compound (11OCB) and one with a bulky tertiary-butyl end-group (*t*-Bu-11OCB), as shown in Fig. 1, which are both known to exhibit only SmA mesophases with similar clearing points, but with significantly different layer spacings.[18] A study of these two compounds essentially enables an assessment of the effect of adding a bulky end-group, and its role in determining the structure of the smectic phase.

We initially present results of temperature-dependent X-ray scattering experiments on the materials, enabling a quantitative characterisation of the SmA phases in terms of their layer spacings and translational order parameters. We then present and analyse fully-atomistic molecular dynamics simulations of the two systems, which provide direct comparisons with the experimental data that enable the observed differences in material properties of these two compounds to be rationalised.

Methods

The syntheses of 11OCB and *t*-Bu-11OCB have been reported previously.[18]

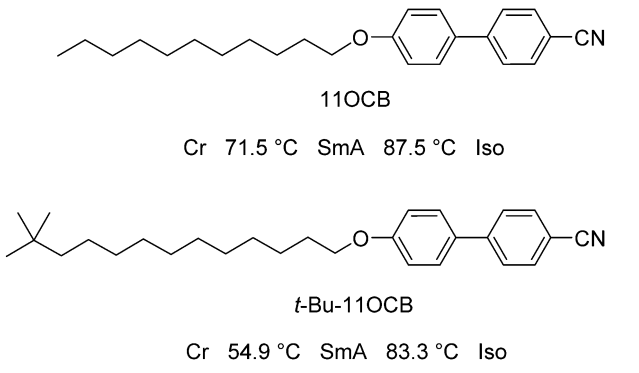

Fig. 1 Structures, names and phase-sequences of the compounds studied in this work.[18]

2D X-ray scattering experiments were performed using a Bruker D8 Discover X-ray diffractometer (λ = 1.5406 Å) with a 2048 × 2048 pixel Bruker VANTEC 500 area detector and a custom-built graphite furnace for temperature control (±0.1 K). Samples were held in borosilicate glass capillaries (0.9 mm outer-diameter) and all scattering patterns were obtained using 180 s scans on cooling of the unaligned samples, with some data recorded in the supercooled regions below the melting points of the compounds. Integrated scattering intensities were fitted using R,[62] and distances determined from X-ray scattering were defined as $\lambda/2\sin\theta$.

Fully atomistic molecular dynamics simulations were performed using GROMACS 5.1.2,[63–69] employing the General Amber Force Field[70] with modifications reported for liquid crystal molecules.[61] Initial topologies were produced using AmberTools 14[71,72] and converted into formats compatible with GROMACS using Acpype.[73] Atomic charges were determined using the RESP method[74] for structures optimised at the B3LYP/6-31G(d) level[75,76] using the Gaussian 09 software package.[77]

Simulations were run using 2 fs steps, with periodic boundary conditions, and with all bonds constrained at their equilibrium lengths using the LINCS algorithm.[78] Trajectory frames were recorded every 50 ps. The temperature of each system was controlled using a Nosé–Hoover thermostat[79,80] and a pressure of 1 bar was maintained using anisotropic Parrinello–Rahman pressure coupling,[81,82] enabling the relative dimensions of the simulation box to vary during each simulation. A van der Waals cut-off of 1.2 nm was employed, and long-range electrostatic interactions were calculated by using the Particle Mesh Ewald method,[83] also with a cut-off of 1.2 nm.

Initial gas-phase density lattices of 1008 molecules were constructed with random head–tail molecular orientations before being compressed over *ca.* 70 ps to a liquid-phase density, resulting in the essentially isotropic starting geometries for the simulations reported here. This method ensured that little of the original order was maintained, providing confidence in the thermodynamic stability of the ordered phases that formed in the simulations reported here.

Second-rank orientational order parameters, P_2, were calculated for each trajectory frame as $-2\times$ the middle eigenvalue of the ordering tensor, $Q_{\alpha\beta}$,[61] defined by eqn (1),[42,84] where N is the number of molecules, j is the molecule number in the simulation, α and β represent the Cartesian x, y and z axes, δ is the Kronecker delta, and a is the component of the principal molecular axis vector defined in the text. The director at each frame was defined as the eigenvector associated with the largest eigenvalue of the ordering tensor.

$$Q_{\alpha\beta} = \frac{1}{N}\sum_{j=1}^{N}\frac{3a_{j\alpha}a_{j\beta} - \delta_{\alpha\beta}}{2} \quad (1)$$

For each trajectory frame, the layer normal was defined using a method described in the literature,[85,86] and was obtained by diagonalising a tensor of local layer normals generated from all N molecules, using an equation equivalent to eqn (1) but with the component of the local layer normal l replacing a. The local

Open Access Article. Published on 11 September 2019. Downloaded on 9/17/2019 10:02:02 AM.
This article is licensed under a Creative Commons Attribution 3.0 Unported Licence.

layer normal at each molecule was determined by selecting a suitable reference position within the molecule, defined in the text, generating a plane by an RMS fit centred on that point and including all equivalent points in other molecules within a cut-off distance of 1 nm, and then calculating the vector normal to this plane.

The MD trajectories were visualised using VMD v1.9.3[87] and Paraview v4.4.0.[88]

Experimental results

Layer spacings

Plots of X-ray scattering intensity against distance are shown across a range of temperatures for both compounds in Fig. 2, along with the layer spacings, d, corresponding to the associated intensity maxima. These results demonstrate that 11OCB has a significantly smaller layer spacing, of *ca.* 3.7 nm, than that of *t*-Bu-11OCB, for which the layer-spacing is *ca.* 4.3–4.4 nm. Both compounds exhibit some contraction of the layer spacing with increasing temperature, and this effect is more pronounced for *t*-Bu-11OCB than for 11OCB. These observations are consistent with previous reported values and trends,[18] which were attributed to the way in which the bulky end-groups are incorporated into the aliphatic region of the smectic layers.

Order parameters

The translational order parameter, τ, provides a means of quantifying translational order in a system,[89] and may take values between 0 for a system with no translational order, and 1 for a system that exhibits perfect layers. The expression given for the translational order parameter in eqn (2) was derived by Leadbetter,[90] relating it to the integrated intensity $I(T)$ of the X-ray peak at temperature T and the theoretical integrated intensity, I_0, that would be obtained from a perfectly layered configuration.

$$\tau^2 = \frac{I(T)}{I_0} \tag{2}$$

One reported analysis method assumes a power-law dependence of the translational order parameter on the reduced temperature of the system, as given by eqn (3), where β is the order parameter exponent and T_c is the superheating limit of the SmA phase in kelvin, and the temperature-dependence of I is given by eqn (4).[91] Fitting the experimental integrated intensities *versus* temperature to eqn (4) enables β, T_c and I_0 to be determined, hence enabling τ to be determined from eqn (2).

$$\tau = \left(1 - \frac{T}{T_c}\right)^{\beta} \tag{3}$$

$$I(T) = I_0\left(1 - \frac{T}{T_c}\right)^{2\beta} \tag{4}$$

The translational order parameters obtained here by this method are plotted against temperature in Fig. 3, and further details, including plots showing the fits and the fitted values, are given in the ESI.† The translational order parameter values of up to 0.78 obtained here for 11OCB are comparable to reported values derived from experimental data for 8OCB, whereas the values of up to 0.89 obtained here for *t*-Bu-11OCB are significantly higher than those reported for many compounds.[91,92]

Bulk alignment of the samples was not readily achieved in the X-ray capillaries, preventing the determination of experimental orientational order parameters of the compounds in this work.

Computational results

Fully atomistic molecular dynamics simulations of 1008 molecules of 11OCB and *t*-Bu-11OCB, respectively, were run at 353 K (79.85 °C), corresponding to a temperature at which both

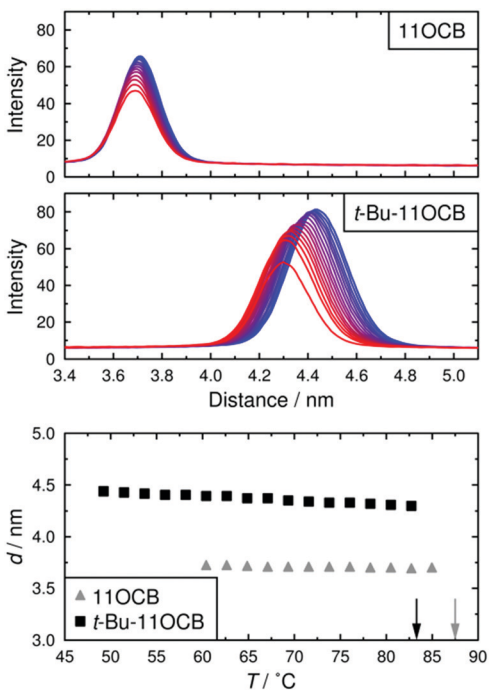

Fig. 2 Plots of scattered X-ray intensity against distance for 11OCB and *t*-Bu-11OCB with decreasing temperature from red to blue (top). The layer spacings corresponding to the intensity maxima are shown plotted against temperature for both compounds (bottom); vertical arrows show the clearing points of the compounds.[18]

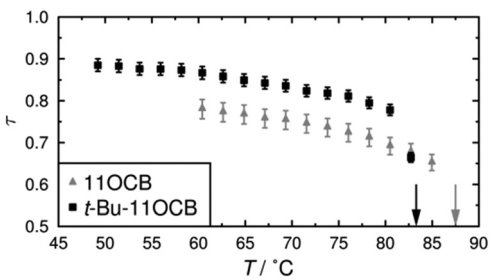

Fig. 3 Translational order parameters, τ, of 11OCB and *t*-Bu-11OCB plotted against temperature. Vertical arrows show the clearing points of the compounds. Error bars correspond to the ranges from 95% confidence intervals for the fitted values of I_0.

This journal is © The Royal Society of Chemistry 2019

Open Access Article. Published on 11 September 2019. Downloaded on 9/17/2019 10:02:02 AM.
This article is licensed under a Creative Commons Attribution 3.0 Unported Licence.

compounds exhibit the SmA phase experimentally. Each simulation was run for >1000 ns after the phase developed.

Orientational order parameters

The presence and determination of orientational order is crucial to confirm the successful simulation of a mesophase. Orientational order in liquid-crystalline systems is typically quantified by the second-rank orientational order parameter, P_2, which is defined in eqn (5) in terms of the angle θ between the principal molecular axis of each molecule and the director, which is the average orientation of the principal molecular axes of all the molecules, and where the angular brackets denote an ensemble average. P_2 takes values of 0 for an isotropic system, and 1 for a system of perfectly ordered molecules.[89]

$$P_2 = \left\langle \frac{3\cos^2\theta - 1}{2} \right\rangle \quad (5)$$

For meaningful results and comparisons, the choice of the principal molecular axis is an important consideration.[93] Our recent simulations have indicated that the surface tensor axis may provide a good approximation of the most aligned molecular axis for cyanobiphenyl and other molecules, but this approach is computationally expensive and was considered prohibitive for the relatively large, long simulations presented here. A more usual and computationally less expensive approach in MD studies is to define the principal molecular axis as either that of the minimum moment of inertia (MOI), or as a vector between two atoms along the rigid core of each molecule.[42,44,94] In the studies reported here, the presence of the heavy tertiary-butyl end-group of *t*-Bu-11OCB means that the minimum MOI axis of this compound will be more influenced by the chain conformation than that of 11OCB. Hence, for the purpose of making a clear comparison using an axis that is consistent between these two molecules, we chose the vector between the N and O atoms as the principal molecular axis. The second-rank orientational order parameters of these axes during the simulations are presented in Fig. 4, which shows that the order for 11OCB develops over *ca.* 100 ns from the start of the simulation, whereas the order develops over a much longer time of *ca.* 1000 ns for *t*-Bu-11OCB and its onset does not occur until *ca.* 300 ns after the start of the simulation. Firm conclusions on the reasons for this difference cannot be drawn from these plots alone, but they do suggest that there are significant differences in the self-assembly of the phases arising from the presence of the additional *t*-Bu group in *t*-Bu-11OCB. The orientational order is maintained at a consistent value after it develops in each simulation, confirming the presence of an ordered phase in each case. The average P_2 values of *ca.* 0.8 for both compounds are consistent with reported values for 11OCB determined from birefringence measurements.[95]

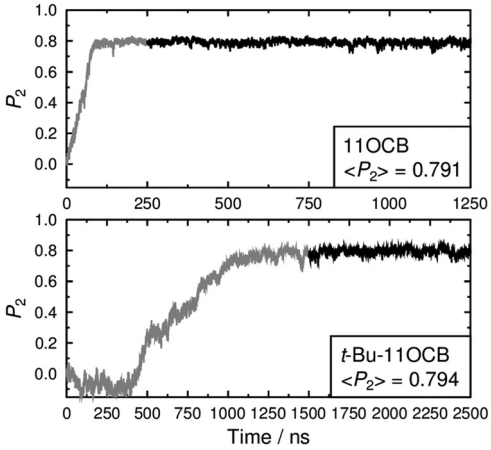

Fig. 4 Orientational order parameters of 11OCB (top) and *t*-Bu-11OCB (bottom) *vs.* time. The average values given in the insets were determined over the last 1000 ns of each simulation, as shown in black.

Translational order parameters

The translational order parameter, τ, was determined for each trajectory frame using the expression given in eqn (6),[43] where L is the length of the box used in the analysis. In this expression, z is the position of an identical point within each molecule that is chosen to represent the molecular position, projected onto the layer normal, which is the average orientation of the local layer normals centred on all of the molecules, d is the overall layer spacing, which is optimised to give the highest value of τ for each trajectory frame, and the angular brackets denote an ensemble average for that frame.

$$\tau = \sqrt{\left[\left\langle \cos\left(\frac{2\pi z}{d}\right)\right\rangle - \frac{d}{2\pi L}\sin\left(\frac{2\pi L}{d}\right)\right]^2 + \left\langle \sin\left(\frac{2\pi z}{d}\right)\right\rangle^2} \quad (6)$$

For trajectory frames which have a non-uniform cross-sectional area of the simulation box along the director, some correction for this variation must be made prior to calculating τ. In reported work,[43] the simulation box was replicated to give a larger cubic cell, within which a cylinder was defined with its long axis parallel to the director, giving a sampling region with uniform cross-section within which the analysis could be carried out. In the work we report here, each contribution to the average terms in eqn (6) was simply divided by the normalised cross sectional area of the simulation box perpendicular to the layer normal at position z, omitting terms for which the cross-sectional area was <10% of the maximum cross-sectional area for the trajectory frame, for which the influence of the correction becomes very large.

Previous studies calculating smectic order parameters from MD simulations have typically used the molecular centre of mass to define the molecular position.[43,56,57] For a perfectly layered configuration of identically aligned molecules, the translational order parameter and layer spacing should be invariant with respect to how the molecular position is defined, providing it is consistent between molecules. However, in some systems, particularly those that exhibit the interdigitated SmA_d phase, such as cyanobiphenyls,[96] the definition of the molecular position may have a significant influence on the calculated translational order parameter and calculated layer spacing. This difference is shown schematically in Fig. 5, where the

Open Access Article. Published on 11 September 2019. Downloaded on 9/17/2019 10:02:02 AM.
This article is licensed under a Creative Commons Attribution 3.0 Unported Licence.

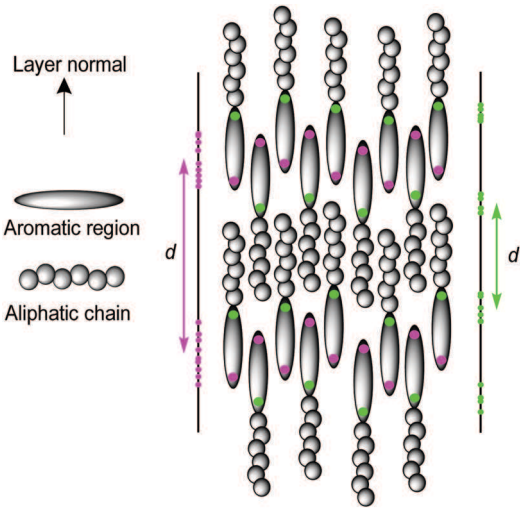

Fig. 5 Schematic representation of the SmA_d phase showing projections (left and right) on to the layer normal for different definitions of the molecular position (shown as magenta and green dots) and their associated layer spacings, *d*.

projections (z) of two different definitions of the molecular position are shown for the same molecular configuration, leading to very different projections of the molecular positions along the layer normal. This difference is particularly relevant for a comparison of 11OCB with *t*-Bu-11OCB, where the bulky end-group in *t*-Bu-11OCB results in a centre of mass in a different position relative to the aromatic core in comparison with that of 11OCB. In this work, the C_4' biphenyl carbon atom, to which the CN group is attached, was found to be the atom in the aromatic region of the molecule with the highest translational order parameter in both systems and it was used to define the molecular positions to calculate the layer normals and values of τ.

The translational order parameters of the C_4' biphenyl atoms along with the associated layer spacings calculated for each trajectory frame are shown in Fig. 6, showing that the translational order in both simulations increases from initial τ values of <0.1 to values of 0.15 and 0.54 for 11OCB and *t*-Bu-11OCB, respectively, determined as averages over the last 1000 ns of each simulation, respectively. Both simulated systems were characterised as SmA phases by analysing the calculated angle between the director and the layer normal for each frame of each simulation, as discussed in the ESI.†

The τ value obtained for 11OCB is very close to that of *ca.* 0.14 reported for united-atom simulations of 8CB,[43] but both are much lower than the respective values derived from experimental data. The significant discrepancy reported between calculated and experimentally derived translational order parameters has been discussed in some detail previously, and has been ascribed to the approximations necessarily applied in deriving the values from experimental data,[43] such as the extrapolation to a hypothetical structure at absolute zero represented by eqn (4).[91]

It can be seen from Fig. 6 that, after the phase has developed, the translational order parameter of *t*-Bu-11OCB is more

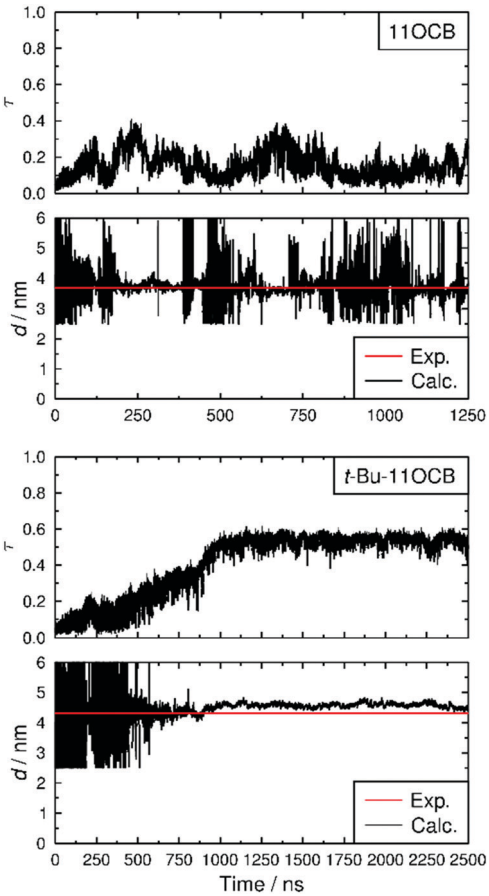

Fig. 6 Translational order parameters, τ, and layer spacings, *d*, determined at each trajectory frame of the MD simulations for 11OCB (top) and *t*-Bu-11OCB (bottom) at 353 K. Experimental values of *d* are shown from the closest temperatures at which the X-ray scattering patterns were recorded (353.65 K).

consistent over the course of the simulation than that of 11OCB. This consistency is likely to be attributable, at least in part, to the higher translational order parameter of *t*-Bu-11OCB, which demonstrates a better defined layer structure that may be less susceptible to fluctuations. This consistency is reflected more strongly in the associated layer spacings of the phases, also shown in Fig. 6, and the contrast in layer structures between the simulations is evident from the snapshots of the equilibrated configurations shown in Fig. 7. The average values of the calculated layer spacings of 3.76 nm and 4.58 nm for 11OCB and *t*-Bu-11OCB, respectively, provide a very close match with the experimental values, with differences of 0.07 nm and 0.27 nm from the measured values of 3.69 nm and 4.31 nm. This match between the calculated and experimental layer spacings further supports the conclusions discussed above, that differences between calculated and experimental translational order parameters may arise from the respective methods used to obtain them.

The close match between the experimental and calculated layer spacings, as well as the match between the trends in the experimental and calculated translational order parameters of these compounds, demonstrates the success of the simulations

This journal is © The Royal Society of Chemistry 2019

Open Access Article. Published on 11 September 2019. Downloaded on 9/17/2019 10:02:02 AM.
This article is licensed under a Creative Commons Attribution 3.0 Unported Licence.

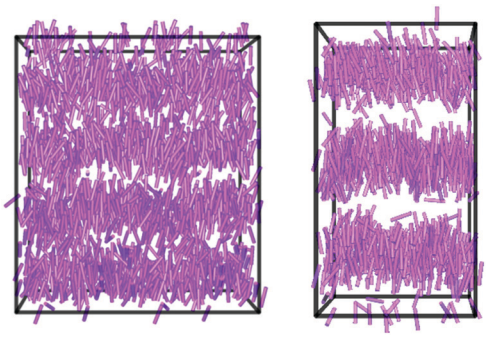

Fig. 7 Snapshots of the simulations of 11OCB at 650 ns (left) and *t*-Bu-11OCB at 2000 ns (right), each shown at a time after equilibration has occurred and with the layer normal oriented vertically. The purple cylinders representing the molecules are drawn between the nitrogen and oxygen atoms, and the boundaries of the simulation boxes are shown in black.

in replicating the general nature of the physical properties of these smectic A phases. The MD trajectories therefore provide a dataset with which the driving forces giving rise to the marked differences in material properties exhibited by these compounds may be assessed.

Molecular interdigitation

Populations of atoms within the 11OCB and *t*-Bu-11OCB molecules along the layer normals were determined for 50 ns windows of each simulation. This analysis window was chosen because the population maxima (*i.e.* layer positions) in both simulations were found to vary by <0.2 nm along the respective layer normals, which is small compared with the layer spacings of *ca.* 4 nm, and thus represents a timescale without significant effects arising from translation of the layers within the simulation box while also providing sufficient data for meaningful analysis. The relative populations of the C_4' biphenyl (head-group) atoms used for the translational order parameter determination, and of the terminal C11 or C13 alkyl (tail-group) atoms of the aliphatic chains, are plotted as black lines in Fig. 8. For both 11OCB and *t*-Bu-11OCB, the populations of these head-group and tail-group atoms are shown to be out of phase, demonstrating the presence of distinct aromatic and aliphatic regions along the layer normals. In comparison with 11OCB, the populations for *t*-Bu-11OCB show sharper peaks with larger amplitudes and greater peak-to-peak separations, along with minima that approach zero between the peaks, all of which is consistent with its higher calculated translational order parameter and wider layer spacing discussed in the previous section. Hence, these plots clearly demonstrate the greater degree of nanosegregation for *t*-Bu-11OCB than 11OCB.

Fig. 8 also shows separate plots for molecules pointing "up" (*i.e.* the vector between the C and N atoms of the CN group has a positive projection on to the layer normal, given by the *z*-axis), and for molecules pointing "down". These plots enable an assessment of the degrees of interdigitation of the molecules from the relative overlaps of the population peaks arising from the up and down molecules.

For the head-group atoms of both 11OCB and *t*-Bu-11OCB there is little difference in the positions of the up and down molecules along the layer normals, demonstrating that there is a significant degree of interdigitation of the aromatic head-groups in both of the simulations. This similarity between the simulations suggests that the nature of the aromatic regions within the layer structures formed by the two compounds is comparable, and therefore that it is unlikely to contribute significantly to the differences in the observed properties of the compounds.

In the case of the tail-group atoms of 11OCB, the relative offsets of the projections of up and down molecules show that there is again little difference between the populations of the up and down molecules, which are comparable to those of the

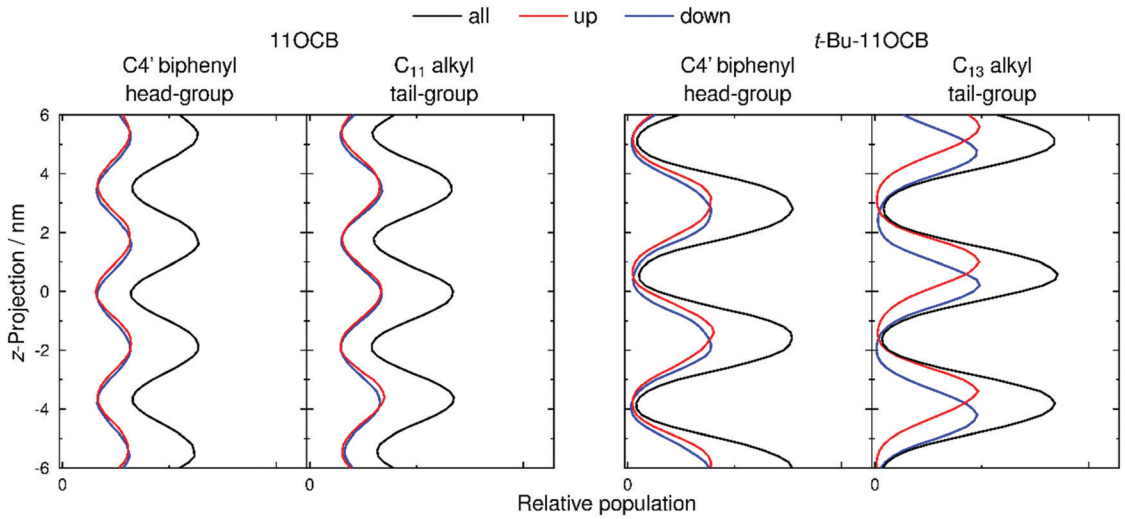

Fig. 8 Relative populations along the layer normal, *z*, of head-group and tail-group atoms for 11OCB and *t*-Bu-11OCB, calculated in the middle 50 ns of the analysis period of each simulation (725–775 ns and 1975–2025 ns, respectively) and generated with 0.2 nm bin-widths. Black lines show the positions for all molecules, whereas red and blue lines represent molecules pointing up and down, respectively. The *z*-projection was defined as zero at the centre of the simulation box and population scales are consistent between plots.

Open Access Article. Published on 11 September 2019. Downloaded on 9/17/2019 10:02:02 AM.
This article is licensed under a Creative Commons Attribution 3.0 Unported Licence.

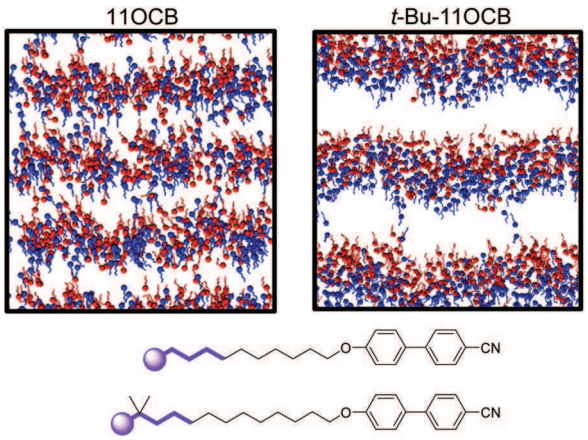

Fig. 9 Views of the final frames of the simulations of 11OCB (left) and *t*-Bu-11OCB (right). Terminal alkyl carbon atoms (C11 and C13, respectively) are shown as spheres, and the next four carbon atoms in the chains are also displayed, as shown in bold on the structures (bottom). Up and down molecules are coloured red and blue, respectively.

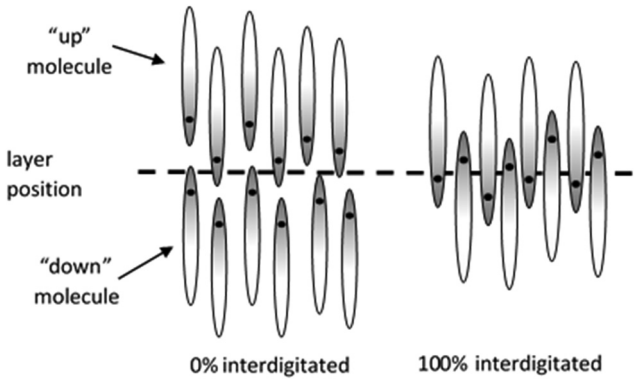

Fig. 10 Schematic representation of quantified molecular interdigitation within smectic layers comprising antiparallel molecules, with the dot indicating the position within the molecule chosen to define the molecular (reference) position.

aromatic head-group atoms. By contrast, the tail-group atoms of *t*-Bu-11OCB show populations of the up and down molecules that are clearly offset along the *z*-axis, indicating that the degree of interdigitation is far lower. This difference suggests that the inter-layer boundary between oppositely oriented molecules is much better defined for *t*-Bu-11OCB than for 11OCB in the aliphatic regions, and a different degree of interdigitation in these regions is also clear from views of the final frame of each simulation given in Fig. 9, in which only the ends of the alkyl chains of the molecules are shown.

For a given definition of the molecular (reference) position, the layer positions may be defined by the population maxima of these molecular positions along the layer normal, as shown by the maxima of the black curves in Fig. 8, and the number of molecules within each layer is given by the total population between the two respective minima along the layer normal. Interdigitation may be defined as occurring when a molecule that is pointing "up" has its reference position below this defined layer position, or when a molecule that is pointing "down" has its reference position above the defined layer position. The degree of interdigitation may then be quantified as the percentage of molecules that show such interdigitation across all the molecules (and layers) in the simulation box. Using this definition, systems that exhibit no overlap of molecular positions corresponding to "up" and "down" molecules within each layer would yield a value of 0%, whereas systems in which all the molecules have their reference positions located beyond those of opposite orientation within each layer would yield a value of 100%, as shown schematically in Fig. 10.

The simulations here give the degree of interdigitation for the head-group atoms as 49% for 11OCB and 50% for *t*-Bu-11OCB, demonstrating significant interdigitation that is very similar between the two materials. For the tail-group atoms, the degree of interdigitation is 47% for 11OCB, similar to that for the head groups of both molecules, whereas it is only 28% for *t*-Bu-11OCB, demonstrating a significantly lower degree of interdigitation at this this end of the molecule.

The carbon atoms comprising the alkyl chains in the two simulations all have the same Lennard-Jones parameters and the sum of the charges of the atoms comprising the end-groups ($-CH_2-CH_2-CH_3$ and $-CH_2-CH_2-{}^tBu$) are within 0.009 between the two molecules. Therefore the tendency of the *t*-Bu groups to separate into discrete layers cannot be attributed to chemical inequivalence, and the significant difference in the nature of the self-organisation of these compounds must therefore be driven by the difference in molecular shape.

The influence of the shape of the bulky end-group in lowering the degree of interdigitation and stabilising the layer structure observed here also provides a consistent picture with the experimental properties reported for cyanobiphenyls with bulky siloxane end-groups, as discussed in the introduction. The marked difference observed and rationalised here, which is attributable to a relatively modest difference in molecular shape, potentially resolves the apparent contradiction between the miscibility of siloxanes with hydrocarbons and their nanosegregation in liquid-crystalline phases.

The separation of the terminal alkyl groups into better defined layers in *t*-Bu-11OCB than 11OCB may also provide a rationale for the greater temperature dependence of the layer spacing in *t*-Bu-11OCB than 11OCB, shown in Fig. 2. In both compounds, the alkyl chains may be expected to favour elongated *trans* conformations as the temperature is reduced, increasing the average molecular lengths. In the case of 11OCB, the small increase in layer spacing on lowering the temperature may arise from any elongation being largely offset by further interdigitation of the chains. For *t*-Bu-11OCB, the larger increase in layer spacing on lowering the temperature may arise from a lower capacity for interdigitation of the bulky *t*-Bu groups to offset any elongation of the chains.

The values quantifying the degrees of interdigitation presented above may also be of significance in the context of the traditional classification of smectic phases, in which the SmA_d phase is typically considered to comprise layers of paired interdigitated molecules.[24] In considering such phases there is a tendency to consider a "unit cell" as comprising only complete molecules, resulting by necessity in there only being one end of the molecule interdigitated, as shown schematically

This journal is © The Royal Society of Chemistry 2019

Open Access Article. Published on 11 September 2019. Downloaded on 9/17/2019 10:02:02 AM.
This article is licensed under a Creative Commons Attribution 3.0 Unported Licence.

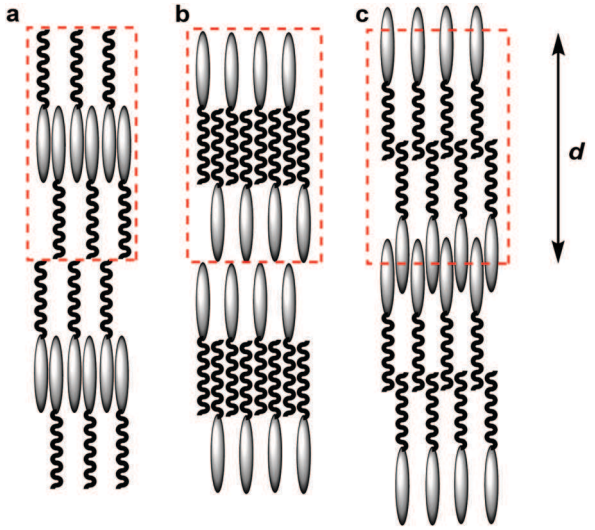

Fig. 11 Schematic illustration of SmA_d phases showing "unit cells" comprising whole molecules showing interdigitation of only one end of the molecules (a and b), and showing interdigitation of both ends of the molecules (c). The layer spacing, *d*, is the same for each representation.

by assemblies (a) and (b) in Fig. 11. Indeed, many studies of cyanobiphenyl compounds have used such models to explain the observed molecular spacing, where either the cyanobiphenyl units or the alkyl chains have been shown to be interdigitated between layers.[25,97–100] The results presented in this work suggest that significant interdigitation may potentially occur between both ends of the molecules, as proposed Leadbetter *et al* in an early model,[101] and as shown schematically by assembly (c) in Fig. 11, and it is the specific structures of these molecular assemblies that underpin the structure of the phase.

In this work, we have shown how the layer structure may be controlled by the size and shape of the alkyl end-group. In general, it would seem that interdigitation may be controlled by interactions between the polar aromatic groups in neighbouring layers and also by interactions between aliphatic chains in neighbouring layers, enabling the properties of layer structures to be tuned through chemically dominated or shape dominated interactions that can be modified at either end of the molecules.

Conclusions

X-ray scattering studies of 11OCB and *t*-Bu-11OCB samples have shown the large difference in smectic layer spacing of the two compounds to be accompanied by a significant difference in their translational order parameters. MD simulations of 11OCB and *t*-Bu-11OCB were shown to replicate absolute experimental layer spacings closely, as well as replicating the trend in translational order parameters between these two compounds. A detailed analysis of interdigitation of the molecules showed that the aromatic regions of the smectic layers were very similar for both compounds, whereas the alkyl regions of the layers differed significantly. The alkyl chains of 11OCB were shown to exhibit a higher degree of interdigitation than those of *t*-Bu-11OCB, which had a tendency to separate into more discrete layers, and this effect is attributed here to the bulky shape of the tertiary-butyl group. The underlying driving force for these differences may be considered to be the layer structure accommodating the molecules in a way that maximises the packing efficiency of the system, thus minimising the free volume;[37] whether this effect is primarily enthalpic, driven by favourable interactions between the molecules, or primarily entropic, driven by the maximisation of the number of accessible states of the system, is the subject of future work.

The effect of bulky end-groups reducing the degree of chain interdigitation may be important to a wide range of materials, given the variety of compounds that have been reported to show behaviour that is similar to those studied here.[18] The results of these simulations also provide strong support for many of the conclusions drawn from experimental work on both these compounds and other smectic materials,[18] showing that the organisation of molecules in the interfaces between the non-polar end-groups is crucial to the nature of the phases formed. The steric effect demonstrated in this work may be expected to be present for any smectic or similar self-organising material comprising molecules with bulky end-groups, and therefore the favourable material properties reported for compounds such as cyanobiphenyls with bulky siloxane end-groups may potentially be exhibited by a wider range of molecules. This potential may provide the opportunity for the rational shape-based design of mesogens with more diverse structural units than those conventionally associated with nanosegregation driven by chemical effects, whilst still retaining favourable material properties.

More generally, the MD studies reported here provide an understanding of the quantitative structure–property relationship at an atomic and molecular level that may open a pathway to the nanoscale engineering of compounds with improved material properties. Such computational studies may be expected to provide an increasingly accessible way of assessing the influence of molecular features on the bulk properties of functional materials.

Conflicts of interest

There are no conflicts to declare.

Acknowledgements

This work was supported by The Engineering and Physical Sciences Research Council (EPSRC) under grant EP/M020584/1 for the development of dyes for liquid crystal applications and the Core Capability grant EP/K039660/1. We thank Dr Richard Mandle for supplying the materials used in this work and Dr Stephen Cowling for experimental assistance. Data from this article are available by request from the University of York Research Database: DOI: 10.15124/42e530cf-ca08-40ce-b182-cdeefe317801.

References

1 W. A. Crossland, A. B. Davey, D. P. Chu and T. V. Clapp, *Handbook of Liquid Crystals*, Wiley-VCH Verlag GmbH & Co. KGaA, 2014, ch. 6, vol. 8, part I, pp. 1–38.

Open Access Article. Published on 11 September 2019. Downloaded on 9/17/2019 10:02:02 AM.
This article is licensed under a Creative Commons Attribution 3.0 Unported Licence.

2 S. T. Lagerwall, *Handbook of Liquid Crystals*, Wiley-VCH Verlag GmbH & Co. KGaA, 2014, ch. 7, vol. 8, part I, pp. 1–24.
3 Y. Yamada and A. Fukuda, *Handbook of Liquid Crystals*, Wiley-VCH Verlag GmbH & Co. KGaA, 2014, ch. 9, vol. 8, part I, pp. 1–40.
4 D. Coates, W. A. Crossland, J. H. Morrisy and B. Needham, *J. Phys. D: Appl. Phys.*, 1978, **11**, 2025–2034.
5 D. J. Gardiner and H. J. Coles, *J. Phys. D: Appl. Phys.*, 2006, **39**, 4948–4955.
6 D. J. Gardiner, C. J. Davenport, J. Newton and H. J. Coles, *J. Appl. Phys.*, 2006, **99**, 113517.
7 Y. Lu, J. Guo, H. Wang and J. Wei, *Adv. Condens. Matter Phys.*, 2012, 843264.
8 H. Y. Chen and J. S. Wu, *J. Soc. Inf. Disp.*, 2010, **18**, 415–420.
9 N. A. Clark and S. T. Lagerwall, *Appl. Phys. Lett.*, 1980, **36**, 899–901.
10 N. M. Abukhdeir and A. D. Rey, *Soft Matter*, 2010, **6**, 1117–1120.
11 I. Dierking, M. Mitov and M. A. Osipov, *Soft Matter*, 2015, **11**, 819–837.
12 D. J. Gardiner and H. J. Coles, *J. Appl. Phys.*, 2006, **100**, 124903.
13 J. P. F. Lagerwall and F. Giesselmann, *ChemPhysChem*, 2006, **7**, 20–45.
14 C. Müller, C. P. J. Schubert, R. P. Lemieux and F. Giesselmann, *ChemPhysChem*, 2018, **19**, 2703–2708.
15 F. Hideo, S. Hiroto, I. Fumito, M. Takeshi, K. Hiroshi, K. Taiichiro and S. Fumio, *Jpn. J. Appl. Phys.*, 2004, **43**, 8161–8167.
16 G. Subramaniam, *Mol. Cryst. Liq. Cryst. Sci. Technol., Sect. A*, 1997, **308**, 121–132.
17 E. Białecka-Florjańczyk, I. Śledzińska, I. Stolarzewicz, A. Makal and E. Górecka, *Liq. Cryst.*, 2009, **36**, 67–73.
18 R. J. Mandle, E. J. Davis, C.-C. A. Voll, D. J. Lewis, S. J. Cowling and J. W. Goodby, *J. Mater. Chem. C*, 2015, **3**, 2380–2388.
19 M. Thompson, C. Carkner, A. Bailey, N. J. Mosey, N. Kapernaum and R. P. Lemieux, *Liq. Cryst.*, 2014, **41**, 1246–1260.
20 M. Thompson, C. Carkner, N. J. Mosey, N. Kapernaum and R. P. Lemieux, *Soft Matter*, 2015, **11**, 3860–3868.
21 S. J. Cowling, A. W. Hall and J. W. Goodby, *Liq. Cryst.*, 2005, **32**, 1483–1498.
22 I. A. Radini and M. Hird, *Liq. Cryst.*, 2009, **36**, 1417–1430.
23 R. J. Mandle, E. J. Davis, J. P. Sarju, N. Stock, M. S. Cooke, S. A. Lobato, S. J. Cowling and J. W. Goodby, *J. Mater. Chem. C*, 2015, **3**, 4333–4344.
24 J. W. Goodby, E. J. Davis, R. J. Mandle and S. J. Cowling, *Handbook of Liquid Crystals*, Wiley-VCH Verlag GmbH & Co. KGaA, 2014, ch. 8, vol. 1, part II, pp. 1–30.
25 A. J. Leadbetter, J. C. Frost, J. P. Gaughan, G. W. Gray and A. Mosley, *J. Phys.*, 1979, **40**, 375–380.
26 M. Ibn-Elhaj, H. J. Coles, D. Guillon and A. Skoulios, *J. Phys. II*, 1993, **3**, 1807–1817.
27 C. Tschierske, *J. Mater. Chem.*, 1998, **8**, 1485–1508.
28 E. Corsellis, D. Guillon, P. Kloess and H. Coles, *Liq. Cryst.*, 1997, **23**, 235–239.
29 T. Murias, A. C. Ribeiro, D. Guillon, D. Shoosmith and H. J. Coles, *Liq. Cryst.*, 2002, **29**, 627–633.
30 W. K. Robinson, C. Carboni, P. Kloess, S. P. Perkins and H. J. Coles, *Liq. Cryst.*, 1998, **25**, 301–307.
31 J. Z. Vlahakis, K. E. Maly and R. P. Lemieux, *J. Mater. Chem.*, 2001, **11**, 2459–2464.
32 M. Ibn-Elhaj, A. Skoulios, D. Guillon, J. Newton, P. Hodge and H. J. Coles, *J. Phys. II*, 1996, **6**, 271–279.
33 H. Yoon, D. M. Agra-Kooijman, K. Ayub, R. P. Lemieux and S. Kumar, *Phys. Rev. Lett.*, 2011, **106**, 087801.
34 L. Li, C. D. Jones, J. Magolan and R. P. Lemieux, *J. Mater. Chem.*, 2007, **17**, 2313–2318.
35 D. J. Gardiner and H. J. Coles, *Proc. Soc. Photo-Opt. Instrum. Eng.*, 2005, **5741**, 239–247.
36 M. V. Gorkunov, M. A. Osipov, N. Kapernaum, D. Nonnenmacher and F. Giesselmann, *Phys. Rev. E: Stat., Nonlinear, Soft Matter Phys.*, 2011, **84**, 051704.
37 J. W. Goodby, R. J. Mandle, E. J. Davis, T. Zhong and S. J. Cowling, *Liq. Cryst.*, 2015, **42**, 593–622.
38 B. Wang and S. Krause, *Macromolecules*, 1987, **20**, 2201–2208.
39 H. Tenhu and K. Vaahtera, *Eur. Polym. J.*, 1991, **27**, 717–722.
40 J. N. Lee, C. Park and G. M. Whitesides, *Anal. Chem.*, 2003, **75**, 6544–6554.
41 M. R. Wilson, *Chem. Soc. Rev.*, 2007, **36**, 1881–1888.
42 J. Pelaez and M. Wilson, *Phys. Chem. Chem. Phys.*, 2007, **9**, 2968–2975.
43 M. F. Palermo, A. Pizzirusso, L. Muccioli and C. Zannoni, *J. Chem. Phys.*, 2013, **138**, 204901.
44 G. Tiberio, L. Muccioli, R. Berardi and C. Zannoni, *ChemPhysChem*, 2009, **10**, 125–136.
45 H. Toriumi, M. Yoshida, N. Kamiya and M. Takeuchi, *Mol. Cryst. Liq. Cryst.*, 2003, **402**, 31–42.
46 Y. Lansac, M. A. Glaser and N. A. Clark, *Phys. Rev. E: Stat., Nonlinear, Soft Matter Phys.*, 2001, **64**, 051703.
47 P. Styring, *Mol. Cryst. Liq. Cryst. Sci. Technol., Sect. A*, 1999, **332**, 199–206.
48 K.-J. Lee, G.-H. Hsiue, J.-L. Wu and J.-H. Chen, *Liq. Cryst.*, 1999, **26**, 469–482.
49 M. Fujiwara, K. Satoh and S. Mita, *Mol. Cryst. Liq. Cryst.*, 2005, **441**, 307–317.
50 F. D. Tsourtou, O. Alexiadis, V. G. Mavrantzas, V. Kolonias and E. Housos, *Chem. Eng. Sci.*, 2015, **121**, 32–50.
51 M. Böckmann, C. Peter, L. D. Site, N. L. Doltsinis, K. Kremer and D. Marx, *J. Chem. Theory Comput.*, 2007, **3**, 1789–1802.
52 A. Pizzirusso, M. Savini, L. Muccioli and C. Zannoni, *J. Mater. Chem.*, 2011, **21**, 125–133.
53 G. D'Avino, L. Muccioli and C. Zannoni, *Adv. Funct. Mater.*, 2015, **25**, 1985–1995.
54 Y. Olivier, L. Muccioli and C. Zannoni, *ChemPhysChem*, 2014, **15**, 1345–1355.
55 I. Cacelli, L. De Gaetani, G. Prampolini and A. Tani, *J. Phys. Chem. B*, 2007, **111**, 2130–2137.
56 L. De Gaetani and G. Prampolini, *Soft Matter*, 2009, **5**, 3517–3526.
57 J. G. Zhang, J. Y. Su and H. X. Guo, *J. Phys. Chem. B*, 2011, **115**, 2214–2227.
58 M. F. Palermo, L. Muccioli and C. Zannoni, *Phys. Chem. Chem. Phys.*, 2015, **17**, 26149–26159.

Open Access Article. Published on 11 September 2019. Downloaded on 9/17/2019 10:02:02 AM.
This article is licensed under a Creative Commons Attribution 3.0 Unported Licence.

59 A. Pizzirusso, M. E. Di Pietro, G. De Luca, G. Celebre, M. Longeri, L. Muccioli and C. Zannoni, *ChemPhysChem*, 2014, **15**, 1356–1367.
60 F. Chami, M. R. Wilson and V. S. Oganesyan, *Soft Matter*, 2012, **8**, 6823–6833.
61 N. J. Boyd and M. R. Wilson, *Phys. Chem. Chem. Phys.*, 2015, **17**, 24851–24865.
62 R: A language and environment for statistical computing (2014) R Foundation for Statistical Computing, Vienna, Austria.
63 M. J. Abraham, T. Murtola, R. Schulz, S. Páll, J. C. Smith, B. Hess and E. Lindahl, *SoftwareX*, 2015, **1–2**, 19–25.
64 S. Páll, M. J. Abraham, C. Kutzner, B. Hess and E. Lindahl, in *Solving Software Challenges for Exascale: International Conference on Exascale Applications and Software, EASC 2014, Stockholm, Sweden, April 2-3, 2014, Revised Selected Papers*, ed. S. Markidis and E. Laure, Springer International Publishing, Cham, 2015, pp. 3–27.
65 S. Pronk, S. Páll, R. Schulz, P. Larsson, P. Bjelkmar, R. Apostolov, M. R. Shirts, J. C. Smith, P. M. Kasson, D. van der Spoel, B. Hess and E. Lindahl, *Bioinformatics*, 2013, **29**, 845–854.
66 B. Hess, C. Kutzner, D. van der Spoel and E. Lindahl, *J. Chem. Theory Comput.*, 2008, **4**, 435–447.
67 D. Van Der Spoel, E. Lindahl, B. Hess, G. Groenhof, A. E. Mark and H. J. C. Berendsen, *J. Comput. Chem.*, 2005, **26**, 1701–1718.
68 E. Lindahl, B. Hess and D. van der Spoel, *Molecular Modeling Annual*, 2001, **7**, 306–317.
69 H. J. C. Berendsen, D. Vanderspoel and R. Vandrunen, *Comput. Phys. Commun.*, 1995, **91**, 43–56.
70 J. Wang, R. M. Wolf, J. W. Caldwell, P. A. Kollman and D. A. Case, *J. Comput. Chem.*, 2004, **25**, 1157–1174.
71 D. A. Case, T. E. Cheatham, T. Darden, H. Gohlke, R. Luo, K. M. Merz, A. Onufriev, C. Simmerling, B. Wang and R. J. Woods, *J. Comput. Chem.*, 2005, **26**, 1668–1688.
72 J. Wang, W. Wang, P. A. Kollman and D. A. Case, *J. Mol. Graphics Modell.*, 2006, **25**, 247–260.
73 A. W. Sousa da Silva and W. F. Vranken, *BMC Res. Notes*, 2012, **5**, 367.
74 C. I. Bayly, P. Cieplak, W. Cornell and P. A. Kollman, *J. Phys. Chem.*, 1993, **97**, 10269–10280.
75 A. D. Becke, *J. Chem. Phys.*, 1993, **98**, 5648–5652.
76 C. T. Lee, W. T. Yang and R. G. Parr, *Phys. Rev. B: Condens. Matter Mater. Phys.*, 1988, **37**, 785–789.
77 M. J. Frisch, G. W. Trucks, H. B. Schlegel, G. E. Scuseria, M. A. Robb, J. R. Cheeseman, G. Scalmani, V. Barone, B. Mennucci, G. A. Petersson, H. Nakatsuji, M. Caricato, X. Li, H. P. Hratchian, A. F. Izmaylov, J. Bloino, G. Zheng, J. L. Sonnenberg, M. Hada, M. Ehara, K. Toyota, R. Fukuda, J. Hasegawa, M. Ishida, T. Nakajima, Y. Honda, O. Kitao, H. Nakai, T. Vreven, J. J. A. Montgomery, J. E. Peralta, F. Ogliaro, M. Bearpark, J. J. Heyd, E. Brothers, K. N. Kudin, V. N. Staroverov, R. Kobayashi, J. Normand, K. Raghavachari, A. Rendell, J. C. Burant, S. S. Iyengar, J. Tomasi, M. Cossi, N. Rega, J. M. Millam, M. Klene, J. E. Knox, J. B. Cross, V. Bakken, C. Adamo, J. Jaramillo, R. Gomperts, R. E. Stratmann, O. Yazyev, A. J. Austin, R. Cammi, C. Pomelli, J. W. Ochterski, R. L. Martin, K. Morokuma, V. G. Zakrzewski, G. A. Voth, P. Salvador, J. J. Dannenberg, S. Dapprich, A. D. Daniels, Ö. Farkas, J. B. Foresman, J. V. Ortiz, J. Cioslowski and D. J. Fox, *Gaussian 09, Revision B.01*, Gaussian Inc., Wallingford, CT, 2009.
78 B. Hess, H. Bekker, H. J. C. Berendsen and J. G. E. M. Fraaije, *J. Comput. Chem.*, 1997, **18**, 1463–1472.
79 S. Nosé, *Mol. Phys.*, 1984, **52**, 255–268.
80 W. G. Hoover, *Phys. Rev. A: At., Mol., Opt. Phys.*, 1985, **31**, 1695–1697.
81 M. Parrinello and A. Rahman, *J. Appl. Phys.*, 1981, **52**, 7182–7190.
82 S. Nosé and M. L. Klein, *Mol. Phys.*, 1983, **50**, 1055–1076.
83 T. Darden, D. York and L. Pedersen, *J. Chem. Phys.*, 1993, **98**, 10089–10092.
84 C. Zannoni, in *Molecular Physics of Liquid Crystals*, ed. G. R. Luckhurst and G. W. Gray, Academic Press, London, 1979, pp. 51–84.
85 I. M. Withers, C. M. Care and D. J. Cleaver, *J. Chem. Phys.*, 2000, **113**, 5078–5090.
86 R. Pecheanu and N. M. Cann, *Phys. Rev. E: Stat., Nonlinear, Soft Matter Phys.*, 2010, **81**, 041704.
87 W. Humphrey, A. Dalke and K. Schulten, *J. Mol. Graphics*, 1996, **14**, 33–38.
88 J. Ahrens, B. Geveci and C. Law, in *Visualization Handbook*, ed. C. R. Johnson, Butterworth-Heinemann, Burlington, 2005, pp. 717–731.
89 C. Zannoni, in *The Molecular Dynamics of Liquid Crystals*, ed. G. R. Luckhurst and C. A. Veracini, Kluwer Academic, Dordrecht, 1994, pp. 11–40.
90 A. J. Leadbetter, in *The Molecular Physics of Liquid Crystals*, ed. G. R. Luckhurst and G. W. Gray, Academic Press, London, 1979, pp. 285–316.
91 N. Kapernaum and F. Giesselmann, *Phys. Rev. E: Stat., Nonlinear, Soft Matter Phys.*, 2008, **78**, 062701.
92 Y. Takanishi, A. Ikeda, H. Takezoe and A. Fukuda, *Phys. Rev. E: Stat., Nonlinear, Soft Matter Phys.*, 1995, **51**, 400–406.
93 M. T. Sims, L. C. Abbott, S. J. Cowling, J. W. Goodby and J. N. Moore, *Phys. Chem. Chem. Phys.*, 2017, **19**, 813–827.
94 M. R. Wilson, *J. Mol. Liq.*, 1996, **68**, 23–31.
95 P. D. Roy, M. K. Das and R. Paul, *Mol. Cryst. Liq. Cryst. Sci. Technol., Sect. A*, 2001, **365**, 607–615.
96 J. W. Goodby, *Handbook of Liquid Crystals*, Wiley-VCH Verlag GmbH & Co. KGaA, 2014, ch. 2, vol. 4, part I, pp. 1–26.
97 J. E. Lydon and C. J. Coakley, *J. Phys. Colloq.*, 1975, **36**, C1-45–C1-48.
98 P. E. Cladis, R. K. Bogardus, W. B. Daniels and G. N. Taylor, *Phys. Rev. Lett.*, 1977, **39**, 720–723.
99 Y. Yamamura, R. Tsuchiya, S. Fujimura, M. Hishida and K. Saito, *J. Phys. Chem. B*, 2017, **121**, 1438–1447.
100 G. G. Alexander, S. M. King, R. M. Richardson and H. Zimmermann, *Liq. Cryst.*, 2010, **37**, 961–968.
101 A. J. Leadbetter, J. L. A. Durrant and M. Rugman, *Mol. Cryst. Liq. Cryst.*, 1977, **34**, 231–235.